Role of Bond Adaptability in the Passivation of Colloidal Quantum Dot Solids
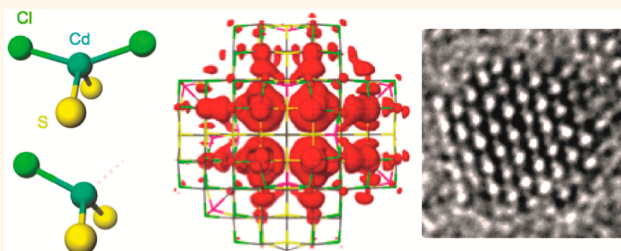
Susanna M. Thon,[†,§] Alexander H. Ip,[†,§] Oleksandr Voznyy,[†] Larissa Levina,[†] Kyle W. Kemp,[†] Graham H. Carey,[†] Silvia Masala,[†,‡] and Edward H. Sargent[†,*]

[†]Department of Electrical and Computer Engineering, University of Toronto, 10 King's College Road, Toronto, Ontario, M5S 3G4, Canada, and [‡]Solar and Photovoltaic Engineering Research Center, King Abdullah University of Science and Technology, 4700 Thuwal, 23955-6900, Saudi Arabia. [§]These authors contributed equally.

ABSTRACT Colloidal quantum dot (CQD) solids are attractive materials for photovoltaic devices due to their low-cost solution-phase processing, high absorption cross sections, and their band gap tunability *via* the quantum size effect. Recent advances in CQD solar cell performance have relied on new surface passivation strategies. Specifically, cadmium cation passivation of surface chalcogen sites in PbS CQDs has been shown to contribute to lowered trap state densities and improved photovoltaic performance. Here we deploy a generalized solution-phase passivation strategy as a means to improving CQD surface management. We connect the effects of the choice of metal cation on solution-phase surface passivation, film-phase trap density of states, minority carrier mobility, and photovoltaic power conversion efficiency. We show that trap passivation and midgap density of states determine photovoltaic device performance and are strongly influenced by the choice of metal cation. Supported by density functional theory simulations, we propose a model for the role of cations, a picture wherein metals offering the shallowest electron affinities and the greatest adaptability in surface bonding configurations eliminate both deep and shallow traps effectively even in submonolayer amounts. This work illustrates the importance of materials choice in designing a flexible passivation strategy for optimum CQD device performance.

KEYWORDS: colloidal quantum dots · photovoltaics · surface passivation · binding energy · DFT · PbS nanocrystals

Colloidal quantum dot (CQD) optoelectronic devices have been the focus of significant research in recent years. CQDs are solution-processed semiconductor nanocrystals compatible with economical roll-to-roll processing methods.[1,2] Additionally, their band gap is readily tuned through control over nanoparticle diameter, a feature that can be exploited in both light-emitting and light-absorbing applications.[3−7] CQD photovoltaic devices have advanced rapidly in performance: since the first demonstration of CQD solar cells in 2005,[8] the power conversion efficiency (PCE) has reached over 7% (certified) in these devices.[9,10]

In addition to the core CQD material chosen (*e.g.*, PbS, CdSe, HgTe, *etc.*), recent reports point increasingly to the crucial importance of controlled incorporation of additional atoms and molecules to enhance the properties of CQD films. Ligand choice has long been known, as expected, to influence electronic transport through the CQD solid,[11−13] both for reasons of passivation and inter-nanoparticle spacing. For instance, mobilities well over 1 cm^2/Vs have been demonstrated in nanocrystal films.[14−17] Additionally, the doping of quantum dots has attracted significant interest recently for development of novel devices such as those leveraging inherently matched quantum junctions and improved potential gradient profiles favoring charge extraction.[18−21] These new devices have been enabled by an enhanced understanding of how overall stoichiometry in the quantum dot solid, taking into account both ligand and nanocrystal material, determines the net doping and electronic properties of the final film.[22,23]

Inorganic strategies based on a complete semiconductor shell surrounding the nanoparticle core have long been pursued.[24−26] Growth of an appropriate shell material has been used to improve luminescence

©2013 American Chemical Society

properties[27] and suppress blinking and Auger recombination.[28−30] Unfortunately, when the goal is excellent passivation combined with superior charge transport, the strategy of employing a thick shell achieves the first but militates against the second priority.

It was recently found that a full shell is not, in fact, necessary to achieve beneficial influence on quantum dot passivation. Early hints of this possibility came in the form of pioneering solution-phase ligand exchanges involving halide adjustment[31,32] as well as investigations of stoichiometry adjustment[33,34] due to the enhanced surface availability and flexibility afforded by solution-phase approaches.

The relevance of inorganic halide passivation to devices and performance came when all-inorganic colloidal quantum dot solids, and solar cells based thereon, were reported in 2011.[35] The joint role of organic bidentate linkers in forming densely packed films, and both cationic and halide inorganic passivants, in achieving lowered trap state densities and improved transport, was proposed, confirmed, and exploited in 2012.[9]

Metal cations on the surface have been shown to have an effect on net nanocrystal surface charge and photoluminescence efficiency.[36] Mechanistically, the role of a submonolayer of inorganics at the surface has been explained *via* its capacity to prevent, or re-form, deep electronic trap states.[37] Interestingly, initial experiment[9] and theory[37] both indicate a role for both the halide, and also for the metal cation, in passivation and thus performance.

In the present work, we sought to build a more thorough understanding of the role of metal cations introduced to the surface of colloidal quantum dots and investigate their impacts on the performance of photovoltaic devices. The work includes a suite of experimental studies in which we vary the identity of the cation and investigate its impact on electronic materials parameters, such as mobility and trap state density, and ultimately on device performance. We finish with a density functional theory (DFT)-based exploration of reasons why the identity of the cation has such a large impact on trap state passivation and consequent device performance.

RESULTS AND DISCUSSION

We focused on inorganic passivation implemented in the solution phase prior to film formation. We took this approach since this process architecture had led to the highest solar cell efficiencies reported to date based on CQDs. Carrying out the treatments in the solution phase offers a high degree of accessibility to the surface by prospective inorganic passivants, maximizing the opportunity to remedy surface trap states.

The approach is depicted in Figure 1. The first portion of the synthesis is standard:[38] a solution of PbO, oleic acid, and octadecene (ODE) is heated to 130 °C

(Figure 1a-i). Rapid injection of bis(trimethylsilyl)sulfide (TMS) in ODE into the flask causes nucleation of PbS quantum dots capped with oleate ligands (Figure 1a-ii). The solution is then allowed to cool while the CQDs grow to the desired size (Figure 1a-iii).

Next is implemented the metal halide treatment that is the subject of this study. During the growth phase, a small volume of a metal chloride (MCl_x) dissolved in oleylamine is rapidly introduced. It has been proposed[9] that chloride ions are able to passivate sites that organic ligands are unable to reach in light of steric hindrance or unfavorable surface topology, thereby reducing surface-associated electronic trap states. This results in CQDs which are capped with both chloride and oleate ligands and which retain colloidal stability.

Metal cations have been reported to incorporate by binding to exposed sulfur atoms on the CQD surface in submonolayer amounts (1−20% relative to Pb).[9,35] The high Pb/S ratio in the as-synthesized CQDs suggests that the surfaces are, by and large, predominantly cation-rich. Thus, the new metal cation is likely replacing the original surface Pb by adsorbing to the surface during growth in lattice sites typically occupied by Pb.[39]

We investigated whether the process might in fact have resulted in a core−shell structure. As seen in TEM (Figure 1b), there is no apparent shell growth on a quantum dot passivated with $CdCl_2$ as previously demonstrated, even as the concentration of metal chloride is increased.[9] We observed no blue shift in the absorption spectrum following addition of the cation precursor (Figure 1c). XPS confirms the incorporation of cations in amounts corresponding to less than 20% of surface Pb sites. There is similarly no significant change in nanocrystal size due to the metal chloride addition, suggestive of self-terminating adsorption to a modest number of relevant surface sites.

Development of the Passivation Strategy. We now describe the development of the metal halide passivation strategy using the prototypical cadmium-based method as an example. In particular, we were interested in learning how the true extent of surface passivation, measured through both luminescence and device performance, was influenced by the incorporation of halide atoms and metal cations. In the suite of treatments explored, we systematically adjusted the concentration of the halide salt in the precursor solution up to the solubility limit (0.86 M) while keeping the volume ratio of the added precursor constant.

The passivation extent in the solution phase was monitored using photoluminescence quantum efficiency (PLQE) measurements. PLQE measured in the solution phase serves as a proxy for the extent of passivation since, in the colloid, the quantum dots are kept well-separated; in contrast, in the film phase, the PLQE is very strongly affected by transport.[40] As seen in Figure 2a, a low concentration of $CdCl_2$
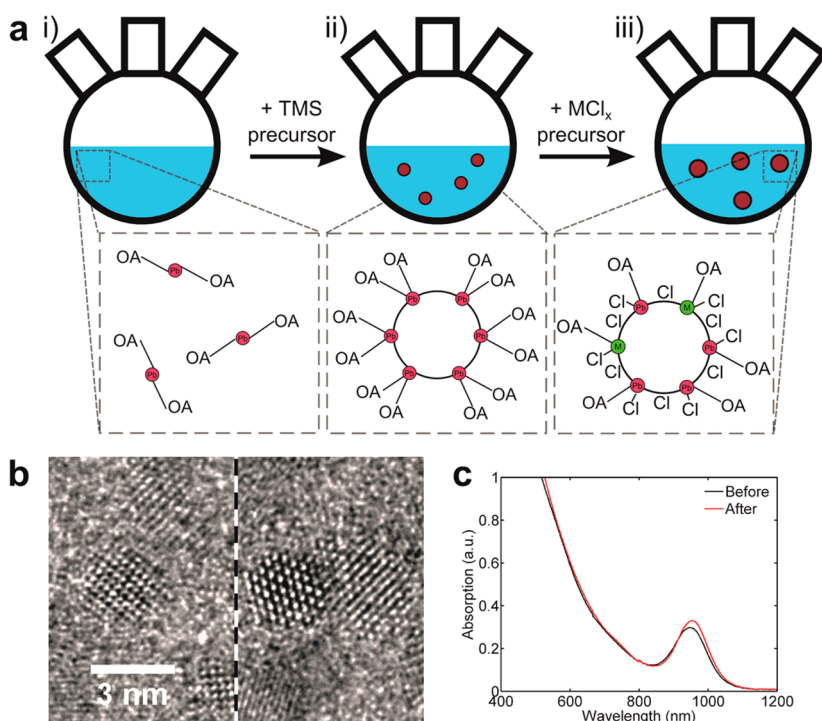
Figure 1. Metal halide passivation of CQDs in solution. (a) CQD synthesis procedure including the metal halide passivation process. (i) Solution of PbO, oleic acid (OA), and ODE is heated to 130 °C. The magnification box depicts lead oleate in solution. (ii) Bis(trimethylsilyl)sulfide (TMS) in ODE is added, causing nucleation of PbS quantum dots capped with oleic acid ligands. The magnification box shows a schematic of a CQD with surface Pb atoms capped with OA. (iii) As the solution cools, 1.0 mL of a solution of MCl$_x$ (where M is a metal cation) in oleylamine is added quickly, typically once the CQD solution reaches a temperature of 80 °C. This results in a partial exchange of oleate for chloride ligands and the incorporation of M cations into the quantum dot surface as seen in the magnification box. (b) TEM images of oleic acid only (left) and metal halide (specifically, 0.3 M cadmium chloride) passivated (right) PbS CQDs showing the same size nanocrystals. The right image shows no evidence of shell formation on the quantum dots. (c) Absorption data of solutions of metal halide passivated and oleic acid only PbS CQDs showing the lack of a spectral shift in peak position.

precursor results in a PLQE of approximately 20%. At cation precursor concentrations of 0.3 M or above, the PLQE is increased to above 30%, indicating a significant enhancement in surface passivation. The PLQE approximately saturates at these precursor concentrations, indicating that in this treatment protocol there is no further benefit from a surface passivation perspective in introducing greater amounts of metal halide precursor. We hypothesize that this is due to a saturation of the surface binding sites available to chlorine anions as the ions are not able to efficiently lead to the removal of bound oleate ligands.[32] Some oleate ligands are likely replaced by chloride ions due to an equilibrium process as the ligands bind and unbind. We note that the specifics of the concentration and surface coverage at which this point of diminishing returns is reached are very likely tied to the details of the strategy, in which a finite quantity of surface sites are accessible to balance passivation and colloidal stability.

We carried out a series of electronic, materials, and photovoltaic device studies using films processed from the same suite of solution-treated samples described above. We used these devices to monitor several film-phase performance metrics as a function of metal

halide precursor concentration, including the limiting (minority) carrier mobility, midgap density of states, and photovoltaic power conversion efficiency. All measurements were performed on photovoltaic devices utilizing the depleted heterojunction architecture.[41] Briefly, CQDs were spin-cast onto a TiO$_2$ electrode on fluoride-doped tin oxide (FTO)-coated glass. The film was treated using a solution of mercaptopropionic acid (MPA) in methanol to exchange any remaining oleate and densify the film,[9] followed by methanol washing. Subsequent CQD layers were cast and ligand-exchanged in a layer-by-layer process until the desired film thickness was achieved. Molybdenum oxide, gold, and silver were deposited on top of the film to contact the device.

With the goal of measuring the photocarrier mobility, we obtained photocurrent transients[41] for devices made from several batches of CQDs employing different metal halide passivation. A 640 nm pulsed diode laser with an illumination density set to approximately 1 sun in intensity (100 mW/cm^2) was used to excite photocarriers in the device. Effective transit times (the time for current to decay to 1/e of the peak value) were obtained as a function of net bias. With knowledge of film thickness, we used transit time *versus* average field
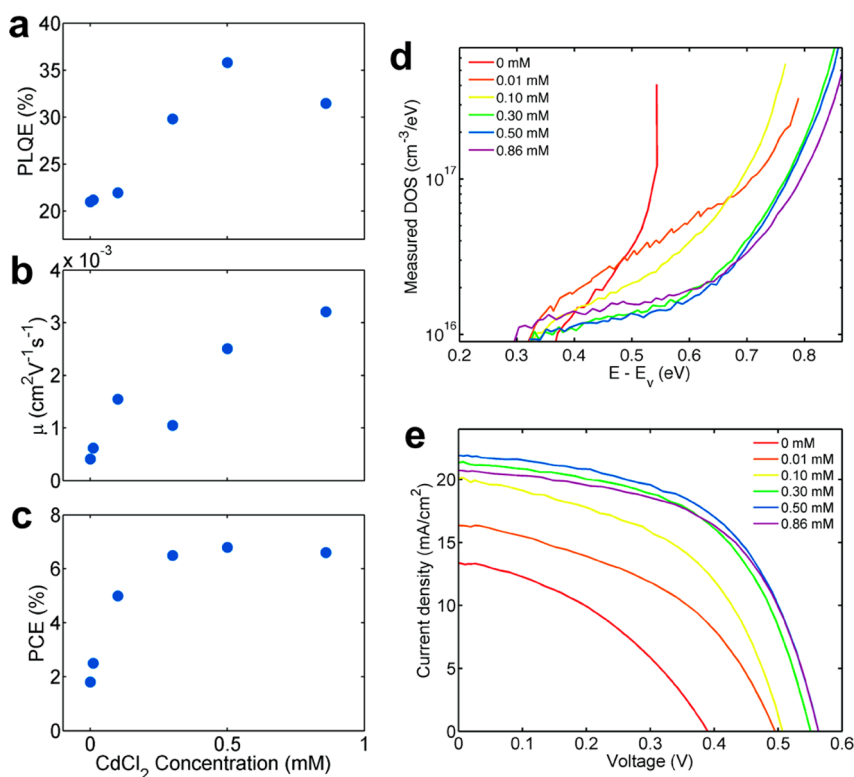
Figure 2. (a) PLQE *vs* CdCl$_2$ precursor concentration showing some saturation with increasing concentration. (b) Mobility *vs* precursor concentration. (c) PCE *vs* precursor concentration shows saturation with concentration, indicating that trap density (as quantified by PLQE and photovoltage transient measurements) plays a more determinative role in device performance than carrier mobility. (d) Density of states for different precursor concentrations determined by photovoltage transient measurements, showing saturation with increasing concentration. (e) Current density−voltage curves for devices made using CQDs with different precursor concentrations of CdCl$_2$.

to extract the limiting carrier mobility for films based on different solution-phase precursor concentrations.

The mobility, calculated using photocurrent transient measurements and plotted in Figure 2b, shows an upward trend relative to increased CdCl$_2$ precursor concentration. This suggests an improvement of transport within the CQD film. Notably, the power conversion efficiency saturates at CdCl$_2$ concentrations above 0.3 M in spite of the increased mobility as shown in Figure 2c. This suggests that the mobility must exceed $\sim 1 \times 10^{-3}$ cm^2/Vs in order for maximum device performance to be obtained, but once this mobility threshold is cleared, another performance-determining mechanism then begins to dominate.

With this in mind, we also characterized the midgap density of states (DOS) in devices fabricated with CQDs utilizing various CdCl$_2$ precursor concentrations (Figure 2d). The DOS was obtained using the photovoltage transient method.[9,42−44] An 830 nm diode laser provides a constant light bias, and a pulsed 640 nm diode laser modulates the open circuit voltage (V_{OC}). By measuring the change in V_{OC} and the total generated charge for each perturbation across a wide range of light bias intensities, we are able to extract the DOS as a function of energetic depth within the band gap of the quantum dot solid.

The results show that the DOS for devices using CQDs with 0.3 M or higher CdCl$_2$ precursor concentration

are all very similar, while lower concentrations clearly show greater DOS deep within the gap. This correlates well with the current density *versus* voltage curves shown in Figure 2e and the PCE saturation behavior seen in Figure 2c. We conclude that further progress in deep trap passivation is the performance-limiting mechanism once the mobility exceeds the 1×10^{-3} cm^2/Vs threshold.

Variation of Film Properties with Cation Passivation Type. Focusing on a single metal chloride, and varying its concentration, we were able to establish the importance of the passivation of deep traps in CQD solids. We sought then to explore how the identity of the metal cation influences passivation and performance.

We screened a wide range of cations with an eye toward maximizing photovoltaic device performance. All of our studies used chlorine as the anionic passivant for consistency and to exclude the effects of varying the anion type on photovoltaic device metrics. We followed the general synthesis optimization procedure described for cadmium above for each of the different metal cations tested. Each cation passivation type was tested with various synthesis conditions. Each of the characterization metrics described in Figure 3 was correlated with device performance for the specific batch, and therefore, some PCE values are different for the same cation in each panel.
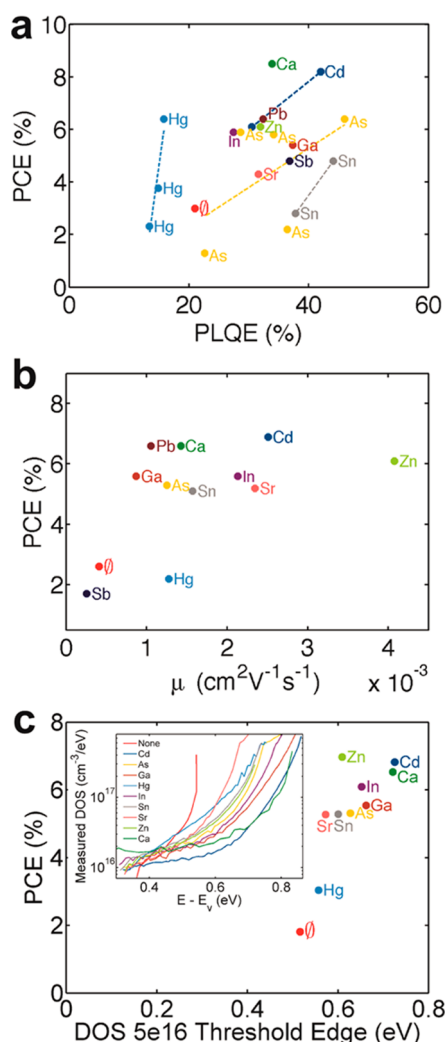
Figure 3. (a) Correlation of PLQE (determined by passivation extent) with device performance. Different batches of CQDs employing the same metal cation passivant under different synthesis conditions show a positive correlation of device performance with PL quantum yield. (b) Mobility for different cation processes determined by photocurrent transient measurements. PCE shows saturation behavior with increasing mobility. (c) Midgap density of states for different cation processes determined by photovoltage transient measurements (inset) and correlation of PCE with DOS threshold edge.

Figure 3 shows the correlation of device performance with solution-phase photoluminescence quantum yield, film mobility and film density of states for the different cation passivation types. As seen in Figure 3a, the device power conversion efficiency is correlated with solution-phase photoluminescence quantum yield, suggestive that the benefits of passivation during solution-phase treatment are at least partially transferred to the final films following the solid-state ligand exchange. Points for slightly different CQD batches utilizing the same metal cation passivant show variation in both PLQE and PCE, and the correlation of PCE with PLQE remains consistent across cation types and is well-correlated for a given cation species, as well, indicating the strong predictive value of this metric.

In contrast, the mobility of charge carriers in films, as measured using the photocurrent transient method,

shows a saturation of power conversion efficiency with increasing mobility for the different cation types, as can be seen in Figure 3b. Cation type has a relatively strong effect on mobility which does not necessarily correlate with photovoltaic device performance. Cation type also has a strong effect on the midgap density of states measured through the photovoltage transient method: in Figure 3c, we plot power conversion efficiency as a function of the open circuit voltage at which a 5×10^{16} cm^{-3}/eV threshold has been reached.

From these studies, it is clear that the midgap density of states is the strong determinant of device performance, and that mobility must simply satisfy a similar threshold to that reported in the CdCl$_2$ study above.

In general, most metal chloride passivation variants produced an increase in device performance compared to CQDs that utilized a solid-state ligand exchange only. The identity of the cation was an important factor, with certain cations—notably Cd, Ca, and Zn—leading to the best device performance. We next sought to understand the origin of this variance to determine the mechanistic source of the improved passivation and performance.

We performed X-ray photoelectron spectroscopy (XPS) measurements to quantify both the amount of chlorine and amount of metal cation incorporated into our quantum dots in the film phase. The variation of power conversion efficiency with anion incorporation extent (measured relative to the amount of lead) for the different processes is presented in Figure 4a. Although the amount of chlorine varied over a relatively large range, the power conversion efficiency saturated with increased chlorine film incorporation. Clearly, some chlorine incorporation is beneficial for device performance, but it does not fully account for the observed variation in efficiency as a function of cation type. The amount of cation incorporation also varies over a wide range for different metal types but displayed no predictive effect on device performance.

This observation suggests that the cation *type* plays an important role in surface passivation, and that even a relatively low concentration of the most desired cations can have a significant beneficial impact. We sought to investigate the role of cation type in surface passivation, for which we turned to DFT simulations.

Using DFT, we calculated the electron affinity of each type of cation that we had tested experimentally. Shallower cation electron affinity is expected to shift the undercoordinated cation dangling bonds deeper into the conduction band, providing better passivation. Simulations of cations adsorbed on the CQD surface were performed, but because of interaction with PbS orbitals, each cation's contribution was observed to spread to a wide range of energies and could not provide a single numerical value to be used as a metric.

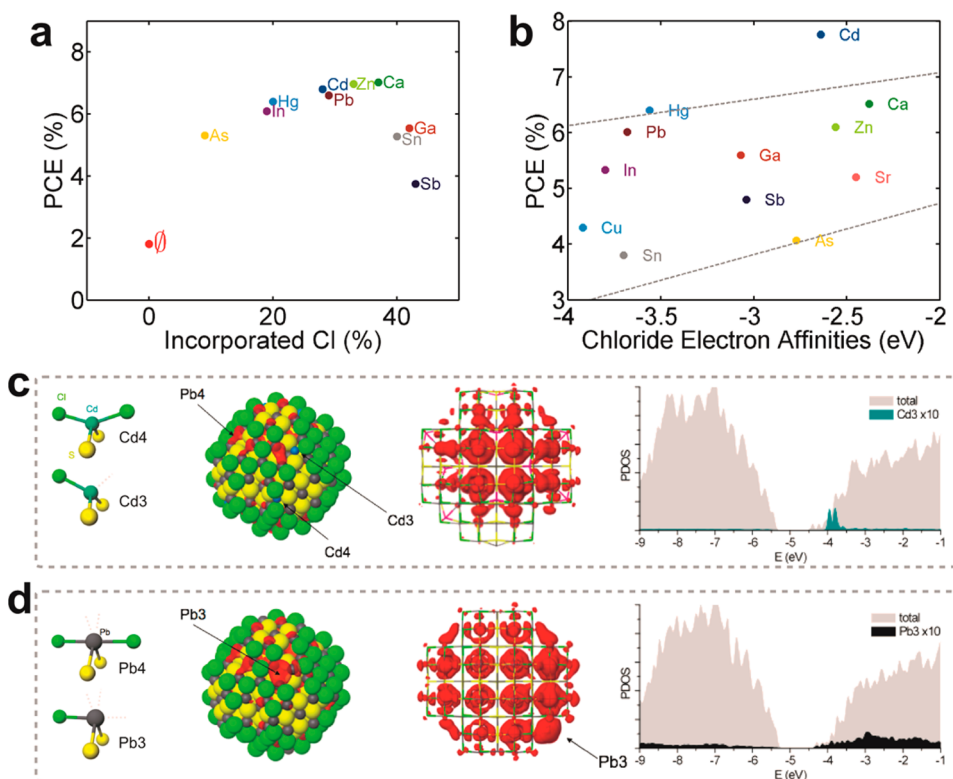We therefore calculated the electron affinities of the corresponding metal chlorides, which we chose to

Figure 4. (a) PCE *vs* chlorine concentration (percentage relative to lead amount) as measured by X-ray photoelectron spectroscopy showing saturation after a certain point. (b) PCE *vs* the electron affinity of the metal chloride molecule calculated *via* density functional theory. There is a weak correlation of PCE with chloride electron affinity. The dotted lines are guides to illustrate the trend. (c) Left to right: binding configuration of Cd on the surface of a PbS CQD with 4 neighbors (top) and 3 neighbors (bottom); the surface of a CQD with Cd incorporated showing that neither Cd-3 nor Cd-4 contributes to conduction band-edge-associated surface states (red); electron density map showing the core-like nature of the conduction band edge states; a density of states plot showing that Cd-associated states are well within the conduction band. (d) Left to right: binding configuration of Pb on the surface of a PbS CQD with 4 neighbors (top) and 3 neighbors (bottom) having more dangling bonds than Cd; the surface of a CQD showing the significant contribution of Pb-3 to the conduction band-edge-associated surface states; electron density map showing the partial surface-like nature of the conduction band edge states; a density of states plot showing the contribution of Pb-associated states to the conduction band edge.

mimic the likely binding configurations of the cations on the CQD surface. The results of the calculations are plotted in Figure 4b. The experimental power conversion efficiency shows a weak correlation with chloride electron affinity. This correlation is maintained even when XPS shows minimal incorporation of the cation itself on the CQD surfaces.

We carried out molecular dynamics simulations on quantum dots with cations bound in several different starting geometries to help explicate this trend further. In particular, we looked at the effect of coordination on the electron wave functions and density of states. The results of calculations for surface cadmium atoms are shown in Figure 4c, and the corresponding results for lead are shown in Figure 4d. Due to the lower ionicity of Cd and the more covalent nature of Cd—S bonds, tetrahedral coordination is preferred over the rocksalt structure. Cadmium is stable on the surface for binding geometries involving 4, 3 (Figure 4c, left), and even 2 neighbors, adopting sp^3, sp^2, and sp orbital hybridizations, respectively. Conversely, the rocksalt structure of PbS requires Pb to have a total of six bonds to be fully coordinated (Figure 4d, left).

Therefore, neither Cd-3 (three-fold coordinated) nor Cd-4 (four-fold coordinated) contributes significantly to the conduction band edge, as can be seen in the density of states plotted in Figure 4c, right, while undercoordinated Pb-4 and Pb-3 contribute significant amplitude to the conduction band edge, and this contribution is in the form of increased surface-like states.

The contribution of certain metal cations to the conduction band edge explains the moderate dependence of device performance on the metal chloride electron affinity. Surface metal chlorides with shallow electron affinities, such as Cd and Ca, contribute states that fall deep within the conduction band (Figure 4c, middle), whereas surface metal chlorides with deep electron affinities such as Pb and Sn can contribute states that fall much closer to the conduction band edge. These states associated with undercoordinated atoms display a partial surface-like character (Figure 4d, middle). Such surface contributions shift the band edge energy, shrinking the band gap. On a CQD film scale, quantum dots with strong surface contributions are responsible for Urbach tails,[33,45] also contributing to broadening of the first absorption peak in

solution. If surrounded by well-passivated dots, a dot with undercoordinated surface atoms would act like a shallow trap and inhibit transport.

We propose the following term to describe this behavior: bond adaptability. Cd can adapt to passivate a wide variety of surface geometries. It can do so without creating partially filled dangling bonds. Cd therefore outperforms Ca, which in spite of having a shallower electron affinity is in fact more ionic, thus requiring six-fold coordination and still contributes to the band edge when it has only three neighbors.

This picture may explain superior photoluminescence quantum yield in solution, where Cd can find and then occupy sites most in need of passivation. Its role is likely of considerably greater importance during the formation of CQD films. The widely employed solid-state ligand exchange is a disruptive process, involving as it does protic attack on the oleate bound to the nanoparticle surface, followed by replacement with the more strongly bound bidentate linker. One can readily envision that some sites of oleate removal could remain unpassivated in the sudden (completed in a matter of a few seconds) MPA treatment, or, worse still, that Pb-oleate could be removed, leaving unpassivated a previously Pb-terminated chalcogen site. An abundance of adaptable Cd in the film may aid in repairing those sites, facets, and geometries most urgently in need of repassivation.

CONCLUSIONS

In summary, this work proposes that bond adaptability can be an important feature of prospective nanoparticle surface passivants. In PbS CQD films, the incorporation of metal cations that can adapt to passivate a variety of surface geometries correlates with superior photovoltaic device performance. These findings illustrate the importance of a multipronged materials approach toward increasing the efficiency of CQD-based optoelectronic devices. Future strategies for increasing CQD photovoltaic device efficiency should concentrate on further reducing the density of midgap recombination centers through consideration of nanocrystal geometry, faceting, and multiple binding motifs in order to ensure complete surface passivation.

METHODS

Device Fabrication. Devices were fabricated on commercially available FTO-coated glass substrates (TEC15, Hartford Glass). To form the n-type electrode, a ZnO nanoparticle solution (NanoShield ZN-2000 diluted to 20% concentration in deionized water) was spin-cast onto the substrates (2500 rpm for 20 s). The substrates were heated to 150 °C for 30 min. Following this, the substrates were immersed in a 120 mM $TiCl_4$ solution and held in an oven at 70 °C for 30 min. Finally, the substrates were dried and annealed on a hot plate at 520 °C for an additional 30 min.

CQD film formation was carried out under atmospheric conditions. To form the CQD film, a 50 mg/mL solution of CQDs in octane was passed through a 0.2 μm filter onto the electrodes and spun at 2500 rpm for 10 s. A 1% v/v solution of 3-mercaptopropionic acid (MPA) in methanol was then used to exchange the oleate ligands. The MPA solution was allowed to sit on the CQD film for 3 s to allow exchange before spinning at 2500 rpm for 5 s. Two rinses with methanol followed to ensure removal of unbound organics. The above process was repeated in a layer-by-layer fashion until the desired thickness was reached (typically 10 layers or ~300 nm). The top electrodes were deposited using an Angstrom Engineering Åmod deposition system integrated in an Innovative Technology glovebox. These contacts consisted of 7.5 nm of thermally evaporated molybdenum oxide, 50 nm electron-beam-deposited gold, and 120 nm of thermally deposited silver.

Photoluminescence Quantum Efficiency Measurements. PLQE was measured by mounting a small amount of CQD solution in a fiber-coupled integrating sphere. A 640 nm diode laser was used to excite the sample, and the photoluminescence and laser signals were collected using near-infrared and visible wavelength range spectrometers, respectively. The PLQE was calculated by taking the integrated difference between the directly excited and indirectly excited photoluminescence photon signals divided by the integrated difference between the direct pump and indirect pump laser photon signals.

AM1.5 Characterization. The device area was properly defined by aperturing[46] to be 0.049 cm^2. Using a xenon lamp and filters (Sciencetech), the solar spectrum at AM1.5 conditions was simulated to within class A specifications. The source intensity was measured using a Melles-Griot broad-band power meter and confirmed using a calibrated reference solar cell (Newport). Current−voltage data were collected using a Keithley 2400 source meter with an estimated accuracy of ±7%.

Colloidal Quantum Dot Synthesis. The PbS nanocrystals were synthesized following a previously published process[38] with or without the addition of a metal chloride precursor solution added during the final cooling stage of synthesis as described in the text. For each metal cation, a concentration range of approximately 0.01 to 1.0 M (or the solubility limit) was explored. The injection of the metal chloride solution typically occurred when the solution reached 80 °C, though it was found that a broad range of temperatures (~50 to 100 °C) could be used. Acetone was used to isolate the cooled PbS nanocrystals followed by centrifugation. The CQDs were dispersed in toluene, precipitated by acetone and methanol in a 1:1 volume ratio mixture, and then washed two or three times with methanol. The final redispersion was done in octane at a concentration of 50 mg/mL.

X-ray Photoelectron Spectroscopy. X-ray photoelectron spectroscopy (XPS, PHI-5500) was used to determine the concentration incorporation of the metal cations and halide anions in the final films in amounts relative to lead. A monochromated Al Kα radiation source (1486.7 eV) was used to excite photoelectrons under ultrahigh vacuum (109 Torr).

Density Functional Theory Calculations. Simulations were performed using the SIESTA software[47] based on pseudopotentials and numerical atomic orbitals as a basis (double-ζ plus polarization quality). The generalized gradient approximation with PBE96 exchange-correlation was used throughout. Scalar-relativistic Troullier−Martins pseudopotentials with nonlinear core corrections were used. Charge density was represented on a grid with 250 Ry cutoff and the GridCellSampling option to effectively double the cutoff for better convergence of forces on atoms. Geometry optimizations were performed until the forces on the atoms converged to below 40 meV/Å. Simulations were performed on a spherical Pb-rich 2.4 nm CQD (~360 atoms in the core) exposing the (100), (110), and (111) facets passivated by Cl as a representative ligand.[37] The electronic imbalance arising from the off-stoichiometry of the dot[22] was compensated by the adsorption of ligands to achieve an undoped CQD.

The use of Cl instead of thiols or carboxylate also allowed for molecular dynamics simulations with a larger time step.

REFERENCES AND NOTES

1. Sargent, E. H. Colloidal Quantum Dot Solar Cells. *Nat. Photonics* **2012**, *6*, 133–135.
2. Graetzel, M.; Janssen, R. A. J.; Mitzi, D. B.; Sargent, E. H. Materials Interface Engineering for Solution-Processed Photovoltaics. *Nature* **2012**, *488*, 304–312.
3. Moreels, I.; Lambert, K.; Smeets, D.; De Muynck, D.; Nollet, T.; Martins, J. C.; Vanhaecke, F.; Vantomme, A.; Delerue, C.; Allan, G.; *et al.* Size-Dependent Optical Properties of Colloidal PbS Quantum Dots. *ACS Nano* **2009**, *3*, 3023–3030.
4. Segets, D.; Lucas, J. M.; Klupp Taylor, R. N.; Scheele, M.; Zheng, H.; Alivisatos, A. P.; Peukert, W. Determination of the Quantum Dot Band Gap Dependence on Particle Size from Optical Absorbance and Transmission Electron Microscopy Measurements. *ACS Nano* **2012**, *6*, 9021–9032.
5. Wang, X.; Koleilat, G. I.; Tang, J.; Liu, H.; Kramer, I. J.; Debnath, R.; Brzozowski, L.; Barkhouse, D. A. R.; Levina, L.; Hoogland, S.; *et al.* Tandem Colloidal Quantum Dot Solar Cells Employing a Graded Recombination Layer. *Nat. Photonics* **2011**, *5*, 480–484.
6. Steckel, J. S.; Coe-Sullivan, S.; Bulović, V.; Bawendi, M. G. 1.3 μm to 1.55 μm Tunable Electroluminescence from PbSe Quantum Dots Embedded within an Organic Device. *Adv. Mater.* **2003**, *15*, 1862–1866.
7. Sun, Q.; Wang, Y. A.; Li, L. S.; Wang, D.; Zhu, T.; Xu, J.; Yang, C.; Li, Y. Bright, Multicoloured Light-Emitting Diodes Based on Quantum Dots. *Nat. Photonics* **2007**, *1*, 717–722.
8. Mcdonald, S. A.; Konstantatos, G.; Zhang, S.; Cyr, P. W.; Klem, E. J.; Levina, L.; Sargent, E. H. Solution-Processed PbS Quantum Dot Infrared Photodetectors and Photovoltaics. *Nat. Mater.* **2005**, *4*, 138–142.
9. Ip, A. H.; Thon, S. M.; Hoogland, S.; Voznyy, O.; Zhitomirsky, D.; Debnath, R.; Levina, L.; Rollny, L. R.; Carey, G. H.; Fischer, A.; *et al.* Hybrid Passivated Colloidal Quantum Dot Solids. *Nat. Nanotechnol.* **2012**, *7*, 577–582.
10. Lan, X.; Bai, J.; Masala, S.; Thon, S. M.; Ren, Y.; Kramer, I. J.; Hoogland, S.; Simchi, A.; Koleilat, G. I.; Paz-Soldan, D.; *et al.* Self-Assembled, Nanowire Network Electrodes for Depleted Bulk Heterojunction Solar Cells. *Adv. Mater.* **2013**, *25*, 1769–1773.
11. Gao, Y.; Aerts, M.; Sandeep, C. S. S.; Talgorn, E.; Savenije, T. J.; Kinge, S.; Siebbeles, L. D. A.; Houtepen, A. J. Photoconductivity of PbSe Quantum-Dot Solids: Dependence on Ligand Anchor Group and Length. *ACS Nano* **2012**, *6*, 9606–9614.
12. Liu, Y.; Gibbs, M.; Puthussery, J.; Gaik, S.; Ihly, R.; Hillhouse, H. W.; Law, M. Dependence of Carrier Mobility on Nanocrystal Size and Ligand Length in PbSe Nanocrystal Solids. *Nano Lett.* **2010**, *10*, 1960–1969.
13. Jeong, K. S.; Tang, J.; Liu, H.; Kim, J.; Schaefer, A. W.; Kemp, K.; Levina, L.; Wang, X.; Hoogland, S.; Debnath, R.; *et al.* Enhanced Mobility-Lifetime Products in PbS Colloidal Quantum Dot Photovoltaics. *ACS Nano* **2012**, *6*, 89–99.
14. Lee, J.-S.; Kovalenko, M. V.; Huang, J.; Chung, D. S.; Talapin, D. V. Band-like Transport, High Electron Mobility and High Photoconductivity in All-Inorganic Nanocrystal Arrays. *Nat. Nanotechnol.* **2011**, *6*, 348–352.
15. Talgorn, E.; Gao, Y.; Aerts, M.; Kunneman, L. T.; Schins, J. M.; Savenije, T. J.; van Huis, M. A.; van der Zant, H. S. J.; Houtepen, A. J.; Siebbeles, L. D. A. Unity Quantum Yield of Photogenerated Charges and Band-like Transport in Quantum-Dot Solids. *Nat. Nanotechnol.* **2011**, *6*, 733–739.
16. Choi, J.-H.; Fafarman, A. T.; Oh, S. J.; Ko, D.-K.; Kim, D. K.; Diroll, B. T.; Muramoto, S.; Gillen, J. G.; Murray, C. B.; Kagan, C. R. Bandlike Transport in Strongly Coupled and Doped Quantum Dot Solids: A Route to High-Performance Thin-Film Electronics. *Nano Lett.* **2012**, *12*, 2631–2638.
17. Chung, D. S.; Lee, J.-S.; Huang, J.; Nag, A.; Ithurria, S.; Talapin, D. V. Low Voltage, Hysteresis Free, and High Mobility Transistors from All-Inorganic Colloidal Nanocrystals. *Nano Lett.* **2012**, *12*, 1813–1820.
18. Zhitomirsky, D.; Furukawa, M.; Tang, J.; Stadler, P.; Hoogland, S.; Voznyy, O.; Liu, H.; Sargent, E. H. N-Type Colloidal-Quantum-Dot Solids for Photovoltaics. *Adv. Mater.* **2012**, *24*, 6181–6185.
19. Ning, Z.; Zhitomirsky, D.; Adinolfi, V.; Sutherland, B.; Xu, J.; Voznyy, O.; Maraghechi, P.; Lan, X.; Hoogland, S.; Ren, Y.; *et al.* Graded Doping for Enhanced Colloidal Quantum Dot Photovoltaics. *Adv. Mater.* **2013**, *25*, 1719–1723.
20. Engel, J. H.; Surendranath, Y.; Alivisatos, A. P. Controlled Chemical Doping of Semiconductor Nanocrystals Using Redox Buffers. *J. Am. Chem. Soc.* **2012**, *134*, 13200–13203.
21. Luther, J. M.; Pietryga, J. M. Stoichiometry Control in Quantum Dots: A Viable Analog to Impurity Doping of Bulk Materials. *ACS Nano* **2013**, *7*, 1845–1849.
22. Voznyy, O.; Zhitomirsky, D.; Stadler, P.; Ning, Z.; Hoogland, S.; Sargent, E. H. A Charge-Orbital Balance Picture of Doping in Colloidal Quantum Dot Solids. *ACS Nano* **2012**, *6*, 8448–8455.
23. Oh, S. J.; Berry, N. E.; Choi, J.-H.; Gaulding, E. A.; Paik, T.; Hong, S.-H.; Murray, C. B.; Kagan, C. R. Stoichiometric Control of Lead Chalcogenide Nanocrystal Solids To Enhance Their Electronic and Optoelectronic Device Performance. *ACS Nano* **2013**, *7*, 2413–2421.
24. Hines, M. A.; Guyot-Sionnest, P. Synthesis and Characterization of Strongly Luminescing ZnS-Capped CdSe Nanocrystals. *J. Phys. Chem.* **1996**, *100*, 468–471.
25. Cao, Y.; Banin, U. Growth and Properties of Semiconductor Core/Shell Nanocrystals with InAs Cores. *J. Am. Chem. Soc.* **2000**, *122*, 9692–9702.
26. Kim, S.; Fisher, B.; Eisler, H.-J.; Bawendi, M. Type II Quantum Dots: CdTe/CdSe(Core/Shell) and CdSe/ZnTe(Core/Shell) Heterostructures. *J. Am. Chem. Soc.* **2003**, *125*, 11466–11467.
27. Pal, B. N.; Ghosh, Y.; Brovelli, S.; Laocharoensuk, R.; Klimov, V. I.; Hollingsworth, J. A.; Htoon, H. 'Giant' CdSe/CdS Core/Shell Nanocrystal Quantum Dots as Efficient Electroluminescent Materials: Strong Influence of Shell Thickness on Light-Emitting Diode Performance. *Nano Lett.* **2012**, *12*, 331–336.
28. Ghosh, Y.; Mangum, B. D.; Casson, J. L.; Williams, D. J.; Htoon, H.; Hollingsworth, J. A. New Insights into the Complexities of Shell Growth and the Strong Influence of Particle Volume in Non-blinking "Giant" Core/Shell Nanocrystal Quantum Dots. *J. Am. Chem. Soc.* **2012**, *134*, 9634–9643.
29. Hollingsworth, J. A. Heterostructuring Nanocrystal Quantum Dots toward Intentional Suppression of Blinking and Auger Recombination. *Chem. Mater.* **2013**, *25*, 1318–1331.
30. Bae, W. K.; Padilha, L. A.; Park, Y.-S.; McDaniel, H.; Robel, I.; Pietryga, J. M.; Klimov, V. I. Controlled Alloying of the Core−Shell Interface in CdSe/CdS Quantum Dots for Suppression of Auger Recombination. *ACS Nano* **2013**, *7*, 3411–3419.
31. Owen, J. S.; Park, J.; Trudeau, P.-E.; Alivisatos, A. P. Reaction Chemistry and Ligand Exchange at Cadmium−Selenide Nanocrystal Surfaces. *J. Am. Chem. Soc.* **2008**, *130*, 12279–12281.

32. Anderson, N. C.; Owen, J. S. Soluble, Chloride-Terminated CdSe Nanocrystals: Ligand Exchange Monitored by ^{1}H and ^{31}P NMR Spectroscopy. *Chem. Mater.* **2013**, *25*, 69–76.

33. Mocatta, D.; Cohen, G.; Schattner, J.; Millo, O.; Rabani, E.; Banin, U. Heavily Doped Semiconductor Nanocrystal Quantum Dots. *Science* **2011**, *332*, 77–81.

34. Bae, W. K.; Joo, J.; Padilha, L. A.; Won, J.; Lee, D. C.; Lin, Q.; Koh, W.; Luo, H.; Klimov, V. I.; Pietryga, J. M. Highly Effective Surface Passivation of PbSe Quantum Dots through Reaction with Molecular Chlorine. *J. Am. Chem. Soc.* **2012**, *134*, 20160–20168.

35. Tang, J.; Kemp, K. W.; Hoogland, S.; Jeong, K. S.; Liu, H.; Levina, L.; Furukawa, M.; Wang, X.; Debnath, R.; Cha, D.; *et al.* Colloidal-Quantum-Dot Photovoltaics Using Atomic-Ligand Passivation. *Nat. Mater.* **2011**, *10*, 765–771.

36. Nag, A.; Kovalenko, M. V.; Lee, J.-S.; Liu, W.; Spokoyny, B.; Talapin, D. V. Metal-Free Inorganic Ligands for Colloidal Nanocrystals: S^{2-}, HS^-, Se^{2-}, HSe^-, Te^{2-}, HTe^-, TeS_3^{2-}, OH^-, and NH_2^- as Surface Ligands. *J. Am. Chem. Soc.* **2011**, *133*, 10612–10620.

37. Voznyy, O.; Thon, S. M.; Ip, A. H.; Sargent, E. H. Dynamic Trap Formation and Elimination in Colloidal Quantum Dots. *J. Phys. Chem. Lett.* **2013**, *4*, 987–992.

38. Hines, M. A.; Scholes, G. D. Colloidal PbS Nanocrystals with Size-Tunable Near-Infrared Emission: Observation of Post-Synthesis Self-Narrowing of the Particle Size Distribution. *Adv. Mater.* **2003**, *15*, 1844–1849.

39. Erwin, S. C.; Zu, L.; Haftel, M. I.; Efros, A. L.; Kennedy, T. A.; Norris, D. J. Doping Semiconductor Nanocrystals. *Nature* **2005**, *436*, 91–94.

40. Zhitomirsky, D.; Voznyy, O.; Hoogland, S.; Sargent, E. H. Measuring Charge Carrier Diffusion in Coupled Colloidal Quantum Dot Solids. *ACS Nano* **2013**, *7*, 5282–5290.

41. Pattantyus-Abraham, A. G.; Kramer, I. J.; Barkhouse, A. R.; Wang, X.; Konstantatos, G.; Debnath, R.; Levina, L.; Raabe, I.; Nazeeruddin, M. K.; Grätzel, M.; *et al.* Depleted-Heterojunction Colloidal Quantum Dot Solar Cells. *ACS Nano* **2010**, *4*, 3374–3380.

42. Li, Z.; Gao, F.; Greenham, N. C.; McNeill, C. R. Comparison of the Operation of Polymer/Fullerene, Polymer/Polymer, and Polymer/Nanocrystal Solar Cells: A Transient Photocurrent and Photovoltage Study. *Adv. Funct. Mater.* **2011**, *21*, 1419–1431.

43. Shuttle, C. G.; O'Regan, B.; Ballantyne, A. M.; Nelson, J.; Bradley, D. D. C.; de Mello, J.; Durrant, J. R. Experimental Determination of the Rate Law for Charge Carrier Decay in a Polythiophene: Fullerene Solar Cell. *Appl. Phys. Lett.* **2008**, *92*, 093311.

44. O'Regan, B. C.; Scully, S.; Mayer, A. C.; Palomares, E.; Durrant, J. The Effect of Al_2O_3 Barrier Layers in TiO_2/Dye/CuSCN Photovoltaic Cells Explored by Recombination and DOS Characterization Using Transient Photovoltage Measurements. *J. Phys. Chem. B* **2005**, *109*, 4616–4623.

45. Guyot-Sionnest, P.; Lhuillier, E.; Liu, H. A Mirage Study of CdSe Colloidal Quantum Dot Films, Urbach Tail, and Surface States. *J. Chem. Phys.* **2012**, *137*, 154704.

46. Snaith, H. J. The Perils of Solar Cell Efficiency Measurements. *Nat. Photonics* **2012**, *6*, 337–340.

47. Soler, J. M.; Artacho, E.; Gale, J. D.; García, A.; Junquera, J.; Ordejón, P.; Sánchez-Portal, D. The SIESTA Method for *Ab Initio* Order-N Materials Simulation. *J. Phys.: Condens. Matter* **2002**, *14*, 2745–2779.

48. Loken, C.; Gruner, D.; Groer, L.; Peltier, R.; Bunn, N.; Craig, M.; Henriques, T.; Dempsey, J.; Yu, C.-H.; Chen, J.; *et al.* SciNet: Lessons Learned from Building a Power-Efficient Top-20 System and Data Centre. *J. Phys. Conf. Ser.* **2010**, *256*, 012026.